Journal of Power Sources 243 (2013) 152–158

Contents lists available at SciVerse ScienceDirect

Journal of Power Sources

journal homepage: www.elsevier.com/locate/jpowsour

Structures and lithium storage performance of Si–O–C composite materials depending on pyrolysis temperatures

Hiroshi Fukui [a,*], Katsuya Eguchi [a], Hisashi Ohsuka [a], Takakazu Hino [a], Kiyoshi Kanamura [b]

[a] Dow Corning Toray Company, Ltd., Kishi, Yamakita 258-0112, Japan
[b] Department of Applied Chemistry, Tokyo Metropolitan University, Minami-Osawa, Hachioji, Tokyo 192-0397, Japan

HIGHLIGHTS

- Pyrolysis of a polysilane/polystyrene blend (700–1200 °C) is reported.
- The Si–O–C composite materials produced at <1200 °C are amorphous in nature.
- The crystalline growth of SiC is observed at 1200 °C.
- Lithium storage performance varies highly depending on pyrolysis temperatures.

ARTICLE INFO

Article history:
Received 3 December 2012
Received in revised form
9 May 2013
Accepted 24 May 2013
Available online 6 June 2013

Keywords:
Silicon oxycarbide
Polysilane
Polystyrene
Pyrolysis
Rechargeable lithium battery
Anode material

ABSTRACT

A polymer blend of a partially-branched phenyl-substituted polysilane, $(Ph_2Si)_{0.85}(PhSi)_{0.15}$, and polystyrene (1:1 by weight) has been prepared to produce silicon oxycarbide (Si–O–C) composite materials through pyrolysis in the temperature range 700–1200 °C under an argon atmosphere. According to elemental analysis results, carbon is a major constituent in a series of Si–O–C composite materials obtained in this study. Completely amorphous features were observed for the composite materials obtained between 700 and 1100 °C, while a clearly discernible crystalline evolution of silicon carbide (SiC) phases was found in a glass network of the composite material obtained at 1200 °C. This paper also deals with electrochemical lithiation and delithiation for the series of Si–O–C composite materials. The first delithiation capacities of these composite materials were highly dependent on pyrolysis temperatures. The composite material obtained at 700 °C had the maximum delithiation capacity of ca. 800 mA h g^{-1}, while the composite material obtained at 1200 °C showed the minimum delithiation capacity of ca. 330 mA h g^{-1}. The crystalline evolution of SiC phases is thought to cause such a drastic decrease in delithiation capacity at 1200 °C.

© 2013 Elsevier B.V. All rights reserved.

1. Introduction

Rechargeable lithium-ion batteries have become essential power sources for a variety of portable electronic devices and recently have started to power electric vehicles on a commercial basis. These applications have been continuously seeking higher-performance lithium-ion batteries that realize a longer operating time and longer-term stability upon charge and discharge cycling. In an attempt to enhance the battery performance, essential changes include a choice of new active materials, which can electrochemically store and release more lithium ions than conventional materials in a reversible way. Therefore, many researches into the discovery of such active materials have been conducted in the battery field [1]. Along with the need for the improvement of cathode materials, a general understanding is that a graphite-based intercalation anode is facing its theoretical capacity limitation up to 372 mA h g^{-1}, which originates from the first-stage structure corresponding to LiC_6 [2]. It would thus be natural that, because of the limitation, research efforts are focused on replacing graphite with new high-capacity anode materials.

It is known that alloying materials have higher gravimetric and volumetric capacities than graphite [1], and in particular, silicon (Si) has been the center of attention as an alternative anode material [3]. For example, a lithiated phase of $Li_{15}Si_4$ yields a gravimetric capacity of ca. 3570 mA h g^{-1} based on the weight of Si [4]. However, its long-cycle stability still appears to be challenging from a practical standpoint. Silicon monoxide (SiO) has also been studied

* Corresponding author. Tel.: +81 465 76 3101; fax: +81 465 75 1064.
E-mail address: h.fukui@dowcorning.com (H. Fukui).

0378-7753/$ – see front matter © 2013 Elsevier B.V. All rights reserved.
http://dx.doi.org/10.1016/j.jpowsour.2013.05.124

as a high-capacity anode material [5]. The structure of SiO characterized by several analytical techniques has been reported to be composed of amorphous SiO_2 and Si [6]. Although the first-cycle coulombic efficiency of SiO is low because of a reaction of SiO_2 and Li to form Si and Li-containing compounds [5], such structural characteristics result in high capacity and relatively good cycling performance with the aid of carbon [7].

Other than Si and SiO, silicon oxycarbide (Si–O–C) glasses are known to offer higher capacities (~920 mA h g^{-1}) than graphite [8]. Si–O–C glasses feature the presence of Si–O and Si–C bonds in a glass network. Therefore, it would be reasonable to suppose that their electrochemical behaviors are quite different from those of Si and SiO. In a previous report we have prepared a Si–O–C composite material that is thought to be composed of graphene layers, micropores, and Si–O–C glass phases, through pyrolysis of a partially-branched phenyl-substituted polysilane, $(Ph_2Si)_{0.85}(PhSi)_{0.15}$ (**1**) and polystyrene (1:1 by weight) at 1000 °C [9]. This composite material showed a high capacity of more than 600 mA h g^{-1} and excellent cyclability, along with intrinsic high rate capability [10]. However, further study is necessary to understand what pyrolysis condition is preferable with respect to electrochemical performance. The work reported herein, therefore, describes how changing pyrolysis temperatures of the polymer blend affects the structures and electrochemical performance of Si–O–C composite materials.

2. Experiments

2.1. Precursor

1 was supplied by Dow Corning Corporation and polystyrene was purchased from Wako Pure Chemical Industries. The details of the polymer precursors have been described elsewhere [9].

2.2. Preparation of the polymer blend

The polymer blend of **1** and polystyrene was prepared in a weight ratio of 1:1, as described elsewhere [9].

2.3. Pyrolysis of the polymer blend

Following the preparation of a char intermediate at 600 °C under a nitrogen atmosphere, further pyrolysis to a final temperature was performed as described elsewhere [9]. Before pyrolysis, the char intermediate was milled and then sieved with a 500 mesh sieve and a 1000 mesh sieve. The char intermediate left on the 1000 mesh sieve was pyrolyzed in a tube furnace in the temperature range 700–1200 °C for 1 h under an argon atmosphere. A heating rate and an argon flow rate were 5 °C min^{-1} and 100 mL min^{-1}, respectively. The nomenclature used for the pyrolysis products is PP-n in this study; PP is the abbreviation for pyrolysis products and n represents pyrolysis temperatures.

2.4. Materials analysis

The char intermediate and the pyrolysis products were characterized by the following techniques. Scanning electron microscopy (SEM) images were collected with a JEOL JSM-6490A (JEOL). X-ray diffraction (XRD) was performed using Cu Kα radiation (1.5418 Å) as the X-ray source (RINT 2200, Rigaku). Raman spectra were recorded on an NRS-1000 spectrometer (JASCO) equipped with a 532-nm green laser source. Elemental analyses (CHN, O, and Si) were performed using an NCH-21 (Sumika Chemical Analysis Service), a Carmhomat 12 ADG (Wösthoff), an EMGA-2800 (Horiba), and an iCAP6500DuoView (Thermo Fisher Scientific). Nitrogen adsorption and desorption isotherms were obtained at 77 K using a Belsorp mini II (BEL JAPAN). The Brunauer–Emmett–Teller (BET) surface areas of the pyrolysis products were determined by using the adsorption isotherms. Unfortunately, there was a difficulty in measuring the isotherms of PP-700 possibly due to contraction at 77 K caused by insufficient carbonization. The BET surface areas of PP-900, PP-1100, and PP-1200 are 9.5, 9.0, and 14 m^2 g^{-1}, respectively. The isotherms were assigned to type-I, which is characteristic of microporous materials, according to the IUPAC classification [11]. These results are comparable to those previously reported for a Si–O–C composite material prepared at 1000 °C [12]. Solid-state ^{29}Si magic angle spinning nuclear magnetic resonance (MAS NMR) analyses were conducted at 59.6 MHz (AC300 spectrometer, Bruker). The detailed procedure has been explained elsewhere [9]. A transmission electron microscopy (TEM) image and a selected area electron diffraction (SAED) pattern for PP-1200 were collected with a JEM-3200FS (JEOL).

2.5. Electrochemical measurements

All electrochemical measurements were undertaken using coin-type (either 2016 or 2032) cells. Prior to cell fabrication in an argon-filled glovebox, the working electrode (14-mm diameter) was prepared by mixing the active material, ketjen black, and poly (vinylidene fluoride) in a weight ratio of 85:7.5:7.5. The powdery mixture dispersed in N-methyl-2-pyrrolidinone (NMP, Wako Pure Chemical Industries) was coated on copper foil. After removal of NMP, the working electrode was cut away from the copper foil. Lithium foil (15-mm diameter, Honjo Metal) was used as the counter electrode. The electrolyte used was a mixture of ethylene carbonate and diethyl carbonate (1:1 by volume) containing 1 mol dm^{-3} $LiPF_6$ (Kishida Chemical). Either a polypropylene or a polyethylene sheet was sandwiched between the working electrode and the counter electrode as a separator. Galvanostatic lithiation and delithiation was conducted at 37.2 mA g^{-1} over two cycles in the voltage range 0–3 V, using a battery cycler (Hokuto Denko, HJ1010mSM8A), at 30 °C. This step is expected to ensure the formation of a solid electrolyte interface (SEI) layer on the surface of the active material. Cycling performance was evaluated at 74.4 mA g^{-1} after the first two cycles under the same condition. After 30 cycles in total, the current density was finally returned to 37.2 mA g^{-1} to evaluate capacity retention.

3. Results and discussion

The pyrolysis summary of the polymer blend is shown in Table 1. An ocher monolith of the char intermediate was produced in 26% yield by thermal decomposition of the polymer blend to 600 °C, showing that its carbonization was not still enough. The char yields after pyrolysis to ≥700 °C all became 95% or higher. It was obvious that the pyrolysis products had changes in color from dark brown at 700 °C to black at ≥800 °C, suggesting further carbonization by increasing pyrolysis temperatures.

Fig. 1a shows the SEM image of the char intermediate obtained at 600 °C. It was found that the char intermediate is made up of different shapes of particles including partially rounded particles and large or sub-micron platelets. Fig. 1b–d shows the SEM images of PP-700, PP-900, and PP-1200. These pyrolysis products have morphology very similar to that of the char intermediate. It appears that the particles are unlikely to vary in size and shape during the course of pyrolysis, remaining almost intact and available for electrode preparation without any further process.

Table 1 also shows the elemental analysis results of the char intermediate and PP-n series. It was found that the char intermediate still contains a large amount of hydrogen atoms probably due

Table 1
Pyrolysis summary and empirical formulas of a char intermediate prepared at 600 °C and pyrolysis products.

Pyrolysis temperature (°C)	Product name	Char yield (%)[a]	Empirical formula of pyrolysis product[b]
600	Char intermediate	26	$SiO_{0.25}C_{8.52}H_{4.76}$
700	PP-700	100	$SiO_{1.17}C_{8.56}H_{3.11}$
900	PP-900	101	$SiO_{0.92}C_{8.23}H_{1.40}$
1100	PP-1100	95	$SiO_{0.41}C_{8.52}H_{0.56}$
1200	PP-1200	95	$SiO_{0.60}C_{8.28}H_{0.57}$

[a] Major weight loss is completed during the course of heat treatment to 600 °C. Char yields after pyrolysis to ≥700 °C may be affected by incompletely-understood characteristics, such as gas adsorption, and thus precise yield calculations may be difficult.
[b] The nitrogen content is not shown because it is negligible.

to its insufficient carbonization. In fact, the content of hydrogen tends to decrease with increasing pyrolysis temperatures. Interestingly, oxygen incorporation appears to have occurred even during the course of heat treatment to 600 °C, and the oxygen-to-silicon ratio increased for the PP-n series depending on pyrolysis temperatures. This might be because the all-phenyl-substituted branched backbone of **1** does not thermally decompose in a way similar to that of methyl-substituted types leading to a Si–C–Si bond formation at ~400 °C [13].

Si–O–C glasses are generally thought to have graphitic carbon, so-called free carbon, thereby creating the need for distinguishing it being not bound to silicon atoms from the other carbon in Si–O–C glass phases. Assuming that the general formula, $SiC_xO_{2(1-x)} + yC_{free}$, can be used for the pyrolysis products, we can estimate the compositions of Si–O–C glass phases and free carbon (Table 2) [14]. The char intermediate and PP-n series were found to be relatively rich in free carbon; y reaches a value of 7.58–8.14. During the course of thermal decomposition, phenyl groups of **1**, in addition to polystyrene, are expected to serve as a free-carbon source. From an electrochemical standpoint, this free carbon may contribute to ensuring electron conductive paths.

Raman spectroscopy is known as a typical method to analyze graphitic carbon structures [15]. In the Raman spectrum of the char intermediate, no peaks were observed, and even PP-700 showed very small Raman peaks in the range 100–2100 cm^{-1}. This would probably be due to the poor growth of graphitic carbon at 600–700 °C. Upon pyrolysis to higher temperatures, on the other hand, there were two broad peaks typical for graphitic carbon in the Raman spectra for PP-900 and PP-1200 (Fig. 2). The G band was observed at ca. 1600 cm^{-1}, while the D band appeared at ca. 1350 cm^{-1} corresponding to the defect of graphitic carbon [15]. According to these results, there was no prominent sign of any discernable structural evolution of graphitic carbon toward a more crystalline form even at 1200 °C.

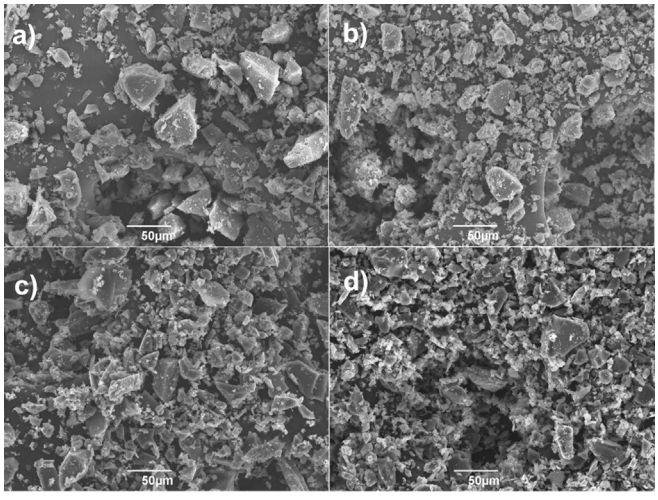

Fig. 1. SEM images of (a) a char intermediate prepared at 600 °C, (b) PP-700, (c) PP-900, and (d) PP-1200.

Table 2
General formulas, $SiC_xO_{2(1-x)} + yC_{free}$, of a char intermediate prepared at 600 °C and pyrolysis products.

Product name	$SiC_xO_{2(1-x)}$[a]	y
Char intermediate	$SiC_{0.88}O_{0.25}$	7.64
PP-700	$SiC_{0.42}O_{1.17}$	8.14
PP-900	$SiC_{0.54}O_{0.92}$	7.69
PP-1100	$SiC_{0.80}O_{0.41}$	7.72
PP-1200	$SiC_{0.70}O_{0.60}$	7.58

[a] $2(1-x)$ is based on the O/Si ratio in each empirical formula.

XRD analysis provides general information on the crystalline structures of the char intermediate and PP-n series. The XRD patterns of the char intermediate and PP-n series are shown in Fig. 3. No sharp peaks were seen in the XRD patterns of the char intermediate and PP-n series (n = 700–1100), showing their completely amorphous natures. A broad peak at 2θ = 21–23° would be composed of the diffractions from both Si–O–C glass phases and graphitic carbon. Another broad peak at 2θ = ca. 43° would be assigned to the (10) diffraction from graphitic carbon. It is obvious that a drastic structural change occurs between pyrolysis to 1100 and 1200 °C. Indeed, PP-1200 shows a shape peak that can readily be discerned at 2θ = ca. 36° in the XRD pattern, along with two other peaks at 2θ = ca. 61° and 72°; these diffraction peaks are thought to be associated with silicon carbide (SiC) phases such as β-SiC [14]. Similar structural evolution has been reported to depend on subtle changes in pyrolysis conditions [14]. Our result also provides evidence that Si–O–C glass phases, if not all, transform into SiC phases. This idea is further supported by TEM/SAED analyses, which indicate the crystalline evolution of SiC phases (Fig. 4). A TEM image was captured for a platelet of PP-1200 (Fig. 4). The inset of Fig. 4 shows the corresponding SAED pattern of PP-1200, where spotty diffraction rings, characteristic of polycrystalline specimens, are identified. Analysis of the SAED pattern suggests that the spotty diffraction rings are attributable to the presence of SiC phases (at ca. 2.5, 1.5, and 1.3 Å). In addition to the spotty diffraction rings, diffuse rings are also visible in the SAED pattern of PP-1200, probably relevant to graphitic carbon and amorphous SiO_2 that could be formed concomitantly with SiC phases [16].

^{29}Si MAS NMR is a useful technique to monitor local changes of silicon environments in Si–O–C glass phases. Fig. 5 shows the ^{29}Si MAS NMR spectra for the char intermediate and PP-n series. The

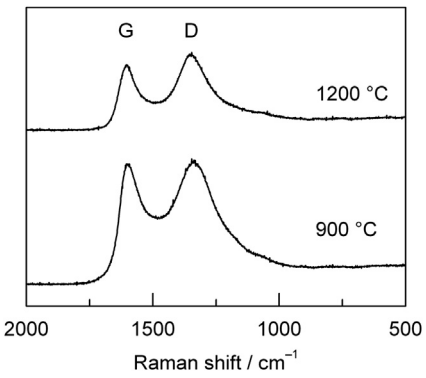

Fig. 2. Raman spectra of (a) PP-900 and (b) PP-1200.

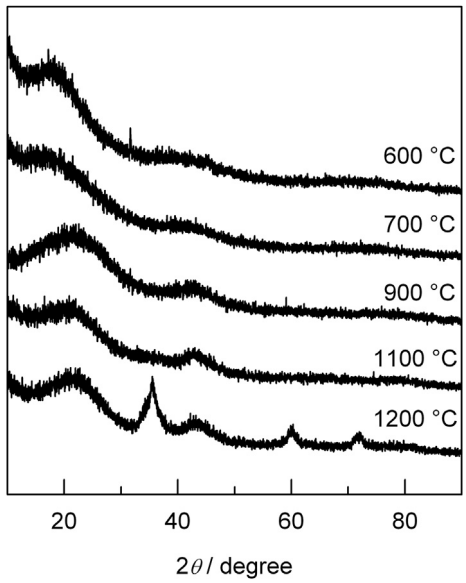

Fig. 3. XRD patterns of a char intermediate prepared at 600 °C and the PP-n series (n = 700–1200).

char intermediate showed a major broad resonance centered at −0.5 ppm along with three minor resonances at −33, −69, and −97 ppm in the ^{29}Si MAS NMR spectrum. Considering that the char intermediate is still likely to be less carbonized with a relatively small amount of oxygen, the major broad resonance could contain some contribution from an SiC_3O unit [14]. The other minor resonances could be assigned to SiC_2O_2, $SiCO_3$, and SiO_4 (Q^3) units [14,17], respectively. The residual hydroxyl groups (Si—OH) in the Q^3 unit should partly be responsible for the presence of hydrogen in the char intermediate, as determined by elemental analysis.

After pyrolysis to 700 °C, a broad resonance dominated at −6.5 ppm in the ^{29}Si MAS NMR spectrum, possibly corresponding to some overlapped contribution from several units such as SiC_3O and SiC_2O_2 with one hydroxyl group [18]. In addition, three minor resonances were still identified at −33, −66, and −99 ppm, respectively. The remaining hydrogen found in PP-700 should also in part originate from hydroxyl groups associated with the −99 ppm resonance. Pyrolysis to 900 and 1100 °C caused a major broad resonance ranging from 20 to −60 ppm to slightly shift to higher field. The other two resonances were seen in the resonance range typical for $SiCO_3$ and SiO_4 (Q^4) units.

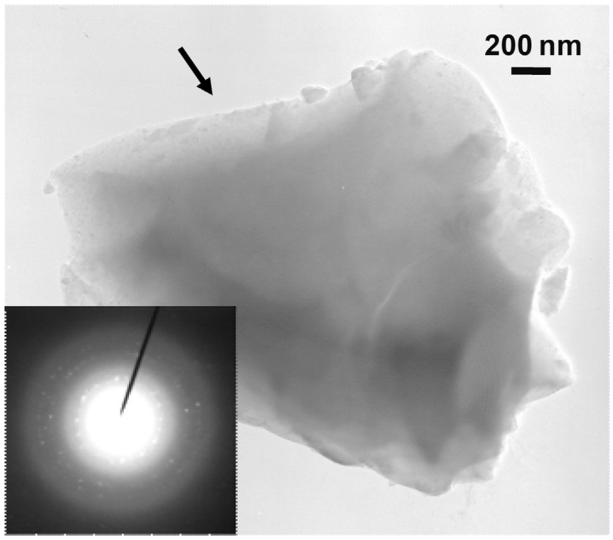

Fig. 4. TEM image and the corresponding SAED pattern of PP-1200.

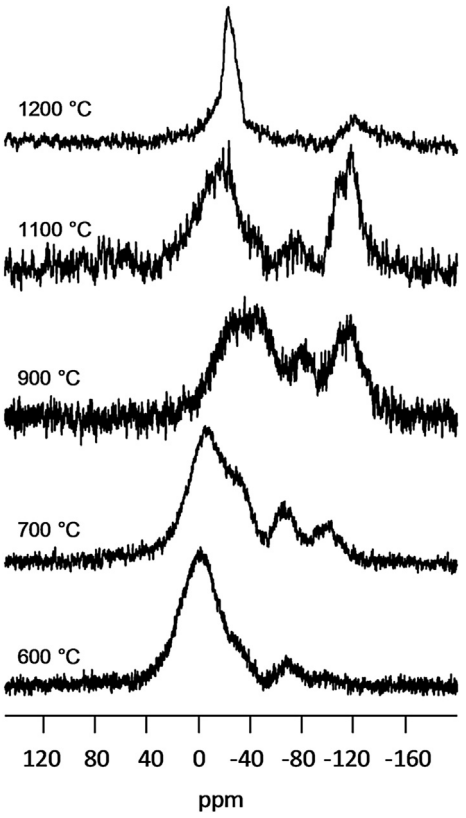

Fig. 5. ^{29}Si MAS NMR spectra of a char intermediate prepared at 600 °C and the PP-n series (n = 700–1200).

A significant structural change can be recognized in the ^{29}Si MAS NMR spectrum after pyrolysis to 1200 °C. A relatively sharp resonance at ca. −24 ppm was observed, indicating that SiC phases became more defined. It has been reported that β-SiC shows a ^{29}Si NMR resonance at ca. −15 ppm [18]. Since the −24 ppm resonance appears to be unsymmetrical, the existence of β-SiC is possible along with α-polytypes [14]. This result is in agreement with that shown in the XRD and TEM/SAED analyses. This structural change can be explained by carbothermic reduction, as observed in pyrolysis of a variety of Si-containing polymeric systems [14,16].

The lithium storage capability of the char intermediate and PP-n series was galvanostatically evaluated with coin-type cells. We summarize the first-cycle lithiation and delithiation results of the char intermediate and PP-n series in Fig. 6. The first lithiation and delithiation capacities were found to be largely dependent on pyrolysis temperatures. The char intermediate showed the first lithiation capacity of 1223 mA h g^{-1} and the first delithiation capacity of 298 mA h g^{-1}. This result thus led to the first coulombic efficiency of 24%. Since the first coulombic efficiency was quite low, it can be said that a majority of lithium ions are irreversibly consumed during the first lithiation. Fig. 7 shows the lithiation and delithiation curves of the char intermediate at the first and the second cycles. Upon the first lithiation, almost all the capacity was observed at 0–0.24 V. Comparison between the first and the second lithiation curve gives insight into a major capacity loss that occurs in the same voltage range. According to our structural analyses, the char intermediate still appears to remain less carbonized, which

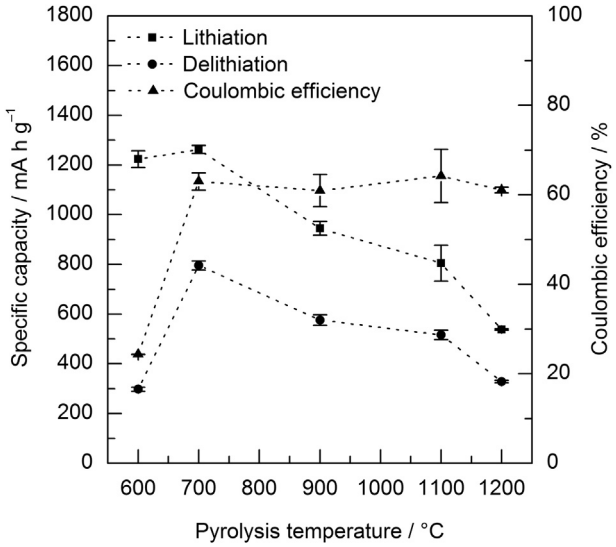

Fig. 6. Lithiation and delithiation capacities and coulombic efficiency at the first cycle depending on pyrolysis temperatures. Note that a pyrolysis temperature of 600 °C corresponds to the performance of a char intermediate prepared at 600 °C.

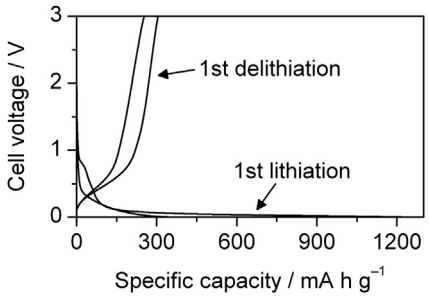

Fig. 7. The first- and second-cycle lithiation and delithiation curves of a char intermediate prepared at 600 °C.

may give rise to such a small delithiation capacity and large irreversible loss of lithium ions, in addition to overvoltage. A minor capacity loss can also be seen at ca. 0.85 V and is probably due to decomposition of the electrolyte to form SEI layers on the surface of the char intermediate. The delithiation capacities were mainly observed below 1.0 V at both the first and the second cycle for the char intermediate.

When n = 700, the first lithiation and delithiation capacities became 1262 and 795 mA h g^{-1}, respectively, thus leading to the first coulombic efficiency of 63% (Fig. 6). We note that PP-700 has the maximum delithiation capacity observed in this study. However, a large irreversible capacity can be seen in the voltage range 0–0.34 V during the first lithiation reaction (Fig. 8a). A new capacity region appeared in the voltage range 0.35–0.5 V upon the second lithiation, suggesting that lithiation pathways are different between the first and the second cycle. A trace for an SEI formation can be recognized at ca. 0.85 V during the first lithiation. According to the second lithiation curve, the main electrochemical lithium storage commences below 0.5 V. On the other hand, it can be seen that the delithiation reactions occur over a wide voltage range. This causes large voltage hysteresis, which is similarly observed for disordered carbon produced from phenolic resin at 700 °C [19]. It is also known that such disordered carbon has its maximum reversible capacity when prepared in the same temperature range [20]. Since PB-700 still possesses much hydrogen, the sp^2-to-sp^3 hybridization change may occur at the edge of graphitic carbon during lithiation, as seen in the case of disordered carbon prepared at 700 °C, leading to such a high capacity and large voltage hysteresis [19].

The first lithiation and delithiation capacities of PB-900 were 945 and 576 mA h g^{-1}, respectively, with the first coulombic efficiency of 61%. PB-900 showed an irreversible capacity probably corresponding to an SEI formation in the voltage range 0.8–0.85 V during the first lithiation reaction (Fig. 8b). Comparison between the first and the second lithiation curve of PB-900 allows for identification of two main stages (0.25–0.6 V and <0.25 V) with respect to irreversible capacity losses. A relatively high content of oxygen could be a cause of the irreversible reactions in PB-900. It is noteworthy that a very short pseudo-voltage plateau appears below 0.2 V in the delithiation curves. This voltage plateau gives us an idea that there would be at least two different electrochemically

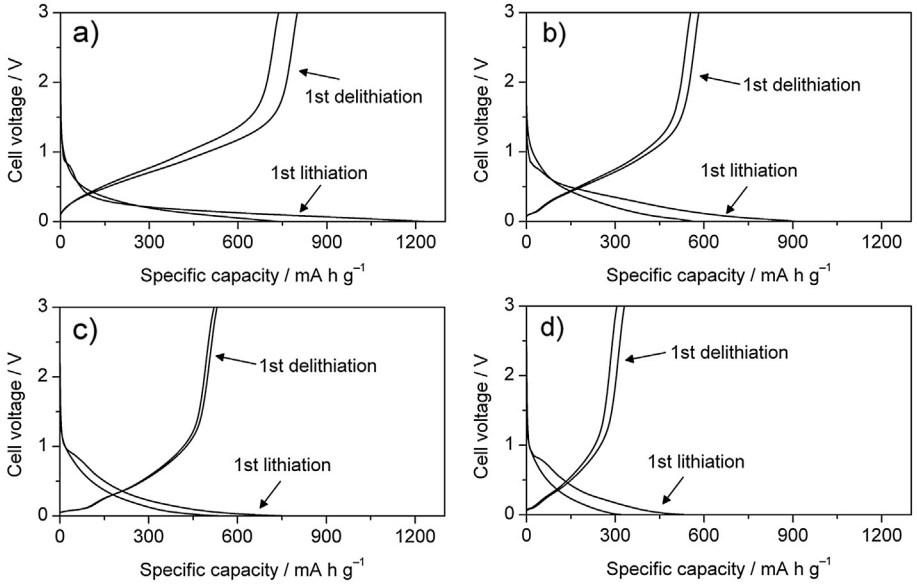

Fig. 8. The first- and second-cycle lithiation and delithiation curves of (a) PP-700, (b) PP-900, (c) PP-1100, and (d) PP-1200.

active sites for lithium storage in PB-900. It is known that hard carbon shows a characteristic voltage plateau in the same voltage range [21]. To explain the emergence of the voltage plateau, it has been proposed that less-ionic lithium species are present in micropores that are formed between misaligned graphene layers [22]. In addition, we have proposed that a Si–O–C composite material, which can be made from the same polymer blend being used in this study and may be regarded here as PP-1000, has micropores where less-ionic lithium species can be stored [9]. It is thus deduced that the formation of micropores begins during the course of pyrolysis between 700 and 900 °C. The delithiation capacities of PB-900 were also observed over a wide range of voltages, as seen in the case of PB-700. Given that PB-900 still contains a relatively large amount of hydrogen, the main reversible capacity may similarly originate from that of disordered carbon [19].

When n = 1100, the first lithiation and delithiation capacities decreased to 805 and 517 mA h g^{-1}, respectively. The first coulombic efficiency thus resulted in 64%, as shown in Fig. 6. In the case of PP-1100, SEI layers likely form at ca. 0.95 V upon the first lithiation (Fig. 8c). A major irreversible capacity region can be seen over a wide range of voltages down to 0 V. Upon delithiation, a pseudo-voltage plateau is clearly visible below ca. 0.1 V for PP-1100, corresponding to a capacity of ca. 100 mA h g^{-1}. PP-1100 is thus thought to have electrochemically active micropores analogous to those previously reported for PP-1000 [9]. The formation of micropores (closed pores) is known to be very susceptible to pyrolysis conditions and possibly change in this temperature range [23]. However, the pseudo-voltage plateau remains and still corresponds to a delithiation capacity of ca. 100 mA h g^{-1}, which is close to that observed for PP-1000 [9]. The measurable decrease in delithiation capacity observed for PP-1100, compared to PP-1000, should thus arise from a partial loss of electrochemically active sites, other than such micropores, rendered by minor structural changes.

It is apparent that PP-1200 suffers from a significant decrease in capacity. Indeed, the first lithiation and delithiation capacities became 538 and 328 mA h g^{-1}, respectively. Compared with PP-1100, the first delithiation capacity of PP-1200 decreased by ca. 37%, with the first coulombic efficiency of 61%. An irreversible reaction, attributed to an SEI formation, likely occurs at ca. 0.8 V upon the first lithiation (Fig. 8d). In a wide voltage range, a major irreversible capacity was observed for PP-1200. The decrease in delithiation capacity should be, in part, due to the fact that a pseudo-voltage plateau can barely be seen below ca. 0.1 V in the delithiation curves. Based on both structural and electrochemical results, the observed SiC evolution is likely accompanied by micropore collapse. It would be reasonable to suppose that drastic structural changes cause such a decrease in delithiation capacity.

Regardless of battery applications, the cycling performance of active materials becomes very important. In this study the cycling performance of PP-700 is of particular interest because of its intrinsic highest lithium storage capacity among the PP-n series. Fig. 9 shows the delithiation capacity of PP-700, PP-900, and PP-1100 over several tens of cycles. It is obvious that PP-700 drastically decreases in delithiation capacity over five cycles. PP-900 and PP-1100 also showed a decrease in delithiation capacity over the initial two cycles. However, the delithiation capacity of these materials tends to become stable in subsequent cycles. We may attribute the capacity decrease observed in common between the second and the third cycle to kinetics and degradation of the active materials and/or the electrodes. In fact, upon decreasing current density (74.4–37.2 mA g^{-1}), all showed an increase in delithiation capacity after 30 cycles. Since, in particular, PP-900 and PP-1100 show a good recovery of delithiation capacities at

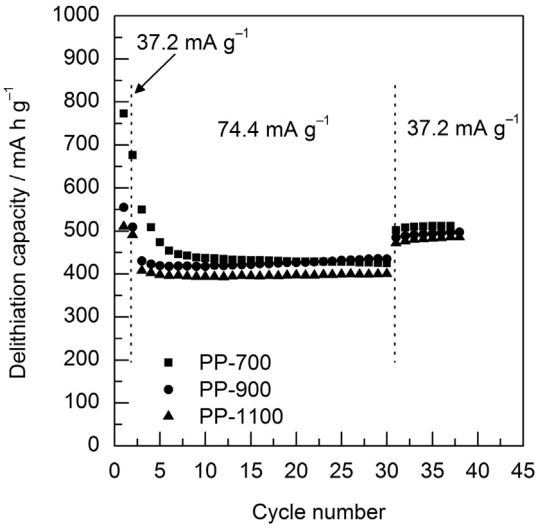

Fig. 9. Cycling performance of PP-700, PP-900, and PP-1100.

37.2 mA g^{-1} after cycling, it would be reasonable to suppose that kinetics is the main cause of such a decrease in delithiation capacity between the second and the third cycle. In the case of PP-700, however, there was a large gap in delithiation capacity between before and after cycling at 74.4 mA g^{-1}. This result represents the occurrence of degradation of PP-700 and/or the electrode to some extent. Considering the fact that the electrodes have not yet been optimized, despite relatively high lithium storage capability, these materials could have long–term cycle stability and thus high potential as an anode material for rechargeable lithium-ion batteries.

4. Conclusion

Following the isolation of a char intermediate obtained from the polymer blend of **1** and polystyrene (1:1 by weight), further pyrolysis to 700–1200 °C was conducted under an argon atmosphere. Structural analyses revealed that the pyrolysis products PP-n (n = 700–1100) are completely amorphous in nature. When n = 1200, the pyrolysis product transformed into a Si–O–C glass containing crystalline SiC phases (PP-1200). Since **1** possesses nothing but phenyl groups and polystyrene also thermally decomposes, excess graphitic carbon (free carbon) is thought to be formed in the PP-n series. Electrochemical measurements showed that PP-700 had the maximum delithiation capacity of ~800 mA h g^{-1}, with large voltage hysteresis between lithiation and delithiation curves. Probably due to the crystalline growth of SiC phases, a drastic decrease in delithiation capacity was observed for PP-1200. A characteristic pseudo-voltage plateau appeared in the early stage of delithiation reactions for PP-900 but not for PP-700. Assuming that the pseudo-voltage plateau is associated with the presence of micropores where less-ionic lithium species can be formed, this pyrolysis temperature range (700–900 °C) is likely to be critical in changing microstructures of the PP-n series, which eventually have an impact on electrochemical lithium storage. In spite of relatively high lithium storage capability, the PP-n series prepared at <1200 °C could have high potential as an anode material, with reasonable capacity retention over several tens of cycles.

Acknowledgments

The authors are grateful to Y. Misaki for TEM/SAED analyses.

References

[1] W.J. Zhang, J. Power Sources 196 (2011) 13–24.
[2] T. Ohzuku, Y. Iwakoshi, K. Sawai, J. Electrochem. Soc. 140 (1993) 2490–2498.
[3] M. Schmuck, A. Balducci, B. Rupp, W. Kern, S. Passerini, M. Winter, J. Solid State Electrochem. 14 (2010) 2203–2207.
[4] D. Mazouzi, B. Lestriez, L. Roué, D. Guyomard, Electrochem. Solid State Lett. 12 (2009) A215–A218.
[5] M. Miyachi, H. Yamamoto, H. Kawai, T. Ohta, M. Shirakata, J. Electrochem. Soc. 152 (2005) A2089–A2091.
[6] K. Schulmeister, W. Mader, J. Non-Cryst. Solids 320 (2003) 143–150.
[7] J.H. Kim, H.J. Sohn, H. Kim, G. Jeong, W. Choi, J. Power Sources 170 (2007) 456–459.
[8] P.E. Sanchez-Jimenez, R. Raj, J. Am. Ceram. Soc. 93 (2010) 1127–1135.
[9] H. Fukui, H. Ohsuka, T. Hino, K. Kanamura, ACS Appl. Mater. Interfaces 2 (2010) 998–1008.
[10] H. Fukui, N. Nakata, K. Dokko, B. Takemura, H. Ohsuka, T. Hino, K. Kanamura, ACS Appl. Mater. Interfaces 3 (2011) 2318–2322.
[11] F. Rouquerol, J. Rouquerol, K. Sing, Adsorption by Powders and Porous Solids, Academic Press, London, 1999.
[12] H. Fukui, H. Ohsuka, T. Hino, K. Kanamura, Chem. Lett. 38 (2009) 86–87.
[13] S. Yajima, J. Hayashi, M. Omori, K. Okamura, Nature 261 (1976) 683–685.
[14] H. Bréquel, J. Parmentier, S. Walter, R. Badheka, G. Trimmel, S. Masse, J. Latournerie, P. Dempsey, C. Turquat, A. Desmartin-Chomel, L. Le Neindre-Prum, U.A. Jayasooriya, D. Hourlier, H.J. Kleebe, G.D. Sorarù, S. Enzo, F. Babonneau, Chem. Mater. 16 (2004) 2585–2598.
[15] M.J. Matthews, M.A. Pimenta, G. Dresselhaus, M.S. Dresselhaus, M. Endo, Phys. Rev. B 59 (1999) 6585–6588.
[16] G.T. Burns, R.B. Taylor, Y. Xu, A. Zangvil, G.A. Zank, Chem. Mater. 4 (1992) 1313–1323.
[17] N. Suyal, D. Hoebbel, M. Mennig, H. Schmidt, J. Mater. Chem. 9 (1999) 3061–3067.
[18] V. Belot, R.J.P. Corriu, D. Leclercq, P.H. Mutin, A. Vioux, J. Non-Cryst. Solids 144 (1992) 287–297.
[19] T. Zheng, W.R. McKinnon, J.R. Dahn, J. Electrochem. Soc. 143 (1996) 2137–2145.
[20] H. Fujimoto, J. Power Sources 195 (2010) 5019–5024.
[21] I. Mochida, C.H. Ku, Y. Korai, Carbon 39 (2001) 399–410.
[22] K. Guérin, M. Ménétrier, A. Février-Bouvier, S. Flandrois, B. Simon, P. Biensan, Solid State Ionics 127 (2000) 187–198.
[23] E. Buiel, A.E. George, J.R. Dahn, J. Electrochem. Soc. 145 (1998) 2252–2257.